Numerical modeling of nonlinear acoustic waves in a tube with an array of Helmholtz resonators

Bruno Lombard, Jean-François Mercier

Numerical modeling of nonlinear acoustic waves in a tube with an array of Helmholtz resonators

Bruno Lombard[a,*], Jean-François Mercier[b]

[a] *LMA, CNRS UPR 7051, Centrale Marseille, Aix-Marseille Univ, F-13402 Marseille Cedex 20, France*
[b] *POEMS, CNRS UMR 7231 CNRS-INRIA-ENSTA, 91762 Palaiseau, France*

Abstract

Wave propagation in a 1-D guide with an array of Helmholtz resonators is studied numerically, considering large amplitude waves and viscous boundary layers. The model consists in two coupled equations: a nonlinear PDE of nonlinear acoustics, and a linear ODE describing the oscillations in the Helmholtz resonators. The dissipative effects in the tube and in the throats of the resonators are modeled by fractional derivatives. Based on a diffusive representation, the convolution kernels are replaced by a finite number of memory variables that satisfy local ordinary differential equations. An optimization procedure provides an efficient diffusive representation. A splitting strategy is then applied to the evolution equations: the propagative part is solved by a standard TVD scheme for hyperbolic equations, whereas the diffusive part is solved exactly. This approach is validated by comparisons with exact solutions. The properties of the full nonlinear solutions are investigated numerically. In particular, existence of acoustic solitary waves is confirmed.

Keywords: nonlinear acoustics, solitons, Burgers equation, fractional derivatives, diffusive representation, time splitting, shock-capturing schemes

*Corresponding author. Tel.: +33 491 16 44 13.
Email addresses: lombard@lma.cnrs-mrs.fr (Bruno Lombard), jean-francois.mercier@ensta.fr (Jean-François Mercier)

1. Introduction

Propagation of linear acoustic waves in lattices has been the object of many theoretical and experimental works. Floquet-Bloch band gaps are exhibited in ordered lattices [4], whereas localization occurs in disordered cases [25]. Nonlinearities, when they are present, are incorporated punctually [26].

Propagation of nonlinear acoustic waves in lattices has been addressed by Sugimoto and his coauthors in a series of theoretical and experimental works [28, 29, 30, 31, 32]. The configuration under study was made up of a tube connected with an array of Helmholtz resonators (figure 1). The latters induce dispersion that competes with the nonlinear effects and may prevent from the emergence of shocks. That is why the original motivation of these works was the reduction of shock waves generated by a high-speed train in a tunnel.

More fundamental questions are also raised, concerning well-known nonlinear waves: the solitons [34, 33]. These ones are stable solitary wave that maintain their shape while they travel at constant speed. Solitons are caused by a cancellation of nonlinear and dispersive effects in the medium. Many physical models yield such solutions, for instance the Korteweg-de Vries equation, the nonlinear Schrödinger equation, and the sine-Gordon equation. In acoustics, dissipation is largely greater than dispersion, so that it was commonly thought that solitary waves were impossible to be generated. But in the Sugimoto's configuration, it was shown that acoustic solitons can exist and propagate in place of shock waves [32].

The model proposed by Sugimoto involves two coupled equations: a nonlinear PDE describing the propagation of large amplitude acoustic waves in the tube, and a linear ODE describing the oscillations in the Helmholtz resonators. The dissipative effects in the tube and in the throats of the resonators are modeled by fractional derivatives [19], that amount to convolution products with singular kernels. A good numerical modeling relies on the following three specifications:

- accurate computation of nonlinear non-smooth waves;
- efficient computation of fractional derivatives, without storing the past values of the solutions;
- stable algorithm under a CFL-like condition, whatever the physical parameters and the amplitude of the waves are.

Figure 1: Guide with an array of Helmholtz resonators (courtesy given by O. Richoux).

The first specification has been well-known for a few decades, based e.g. on shock-capturing schemes [15]. The second requirement is much less standard. Here we follow a strategy relying on the diffusive representation of fractional operators [35, 18, 10, 8, 6, 1]. The fractional derivatives are replaced by a set of memory variables that satisfy local-in-time linear differential equations. The coefficients of this representation are issued from an optimization procedure, which ensures a minimal computational cost of the fractional derivatives. Lastly, the stability specification requires an adequate coupling between the PDE and the ODE. A naive coupling between these equations usually ensures an increase of discrete energy. Here we obtain a stable scheme under the optimal CFL condition.

The paper is organized as follows. The Sugimoto's model is presented in section 2. Dispersion analysis in the linear case is developed, and degeneracy towards Korteweg-de Vries equations is precised. The diffusive representation of fractional derivatives is described in section 3, leading to a first-order system of PDE. The procedure to compute weights and nodes of this representation is explained. The numerical methods are detailed in section 4: a splitting to ensure an optimal CFL condition and to take advantage of efficient methods; a TVD scheme for the advection-Burgers PDE; and an exact resolution of the diffusive part. Numerical experiments are proposed in section 5. Four tests are addressed, concerning successively nonlinear acoustics in the tube, oscillations in the resonators, and the coupling (linear

and nonlinear) between the two subsystems. Numerical measures on the full nonlinear system confirm the classical propertie s of solitons. Conclusion and future directions of research are sketched in section 6.

2. Physical modeling

2.1. Notations

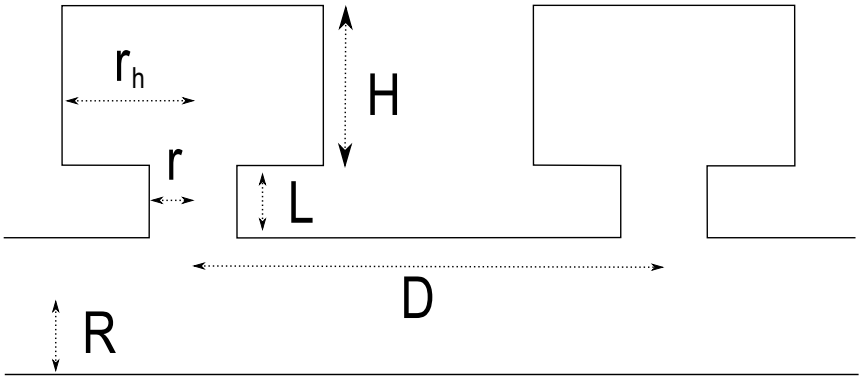

Figure 2: Sketch of the guide with an array of Helmholtz resonators.

The configuration under study is made up of an air-filled tube connected with an array of Helmholtz resonators (figure 2). The cylindrical resonators are uniformly distributed along the tube. The geometrical parameters are the length of the tube $\mathcal{L}$; the radius of the guide R; the axial spacing between resonators D; the radius of the throat r; the length of the throat L; the radius of the cavity r_h; and the height of the cavity H, which may vary depending on the resonator. It follows the cross-sectional area of the guide $A = \pi\, R^2$ and of the throat $B = \pi\, r^2$, the volume of each resonator $V = \pi\, r_h^2\, H$, and the reduced radius:

$$R^* = \frac{R}{1 - \dfrac{R}{2\,D}\,\dfrac{B}{A}} = \frac{R}{1 - \dfrac{r^2}{2\,D\,R}}. \tag{1}$$

The physical parameters are the ratio of specific heats at constant pressure and volume γ; the pressure at equilibrium p_0; the density at equilibrium ρ_0; the Prandtl number Pr; the kinematic viscosity ν; and the ratio of shear and bulk viscosities μ_v/μ. It follows the linear sound speed a_0, the sound

diffusivity ν_d, the dissipation in the boundary layer C, the natural angular frequency of the resonator ω_0 and the natural angular frequency of the tube coupled with the resonator ω_1:

$$\begin{aligned} a_0 &= \sqrt{\frac{\gamma\, p_0}{\rho_0}}, \qquad \nu_d = \nu\left(\frac{4}{3} + \frac{\mu_v}{\mu} + \frac{\gamma-1}{\mathrm{Pr}}\right), \qquad C = 1 + \frac{\gamma-1}{\sqrt{\mathrm{Pr}}}, \\ \omega_0 &= a_0\sqrt{\frac{B}{L\,V}} = a_0\,\frac{r}{r_h}\frac{1}{\sqrt{L\,H}}, \qquad \omega_1 = \omega_0\sqrt{1+\frac{V}{2\,A\,D}}. \end{aligned} \tag{2}$$

Under a one-dimensional assumption, the variables are the axial velocity of the gas u and the excess pressure in the cavity p (denoted $p_2^{'} = p_2 - p_0$ in the papers of Sugimoto, p_2 being the pressure in the cavity of the resonators). The wavelength of the initial disturbance is λ. It follows the acoustic Mach number M, the parameter of nonlinearity ε, the characteristic angular frequency ω, the excess pressure $p^{'}$ in the tube (in the linear theory) and the intensity of sound I (in dB):

$$\begin{aligned} M &= \frac{u}{a_0}, \qquad \varepsilon = \frac{\gamma+1}{2}\,M, \qquad \omega = \frac{2\,\pi\,a_0}{\lambda}, \\ \frac{p^{'}}{p_0} &= \gamma\frac{u}{a_0}, \qquad I = 20\,\log\left(\frac{2\,\gamma}{\gamma+1}\,\frac{p_0}{p_{ref}}\,\varepsilon\right), \end{aligned} \tag{3}$$

where $p_{ref} = 2\,10^{-5}$ Pa.

2.2. Governing equations

The main assumptions underlying Sugimoto's model are [29]:

- 1D geometry;
- weak acoustic nonlinearity in the tube ($\varepsilon \ll 1$);
- continuous distribution of resonators ($\lambda \gg D$);
- no interactions between neighboring resonators ($\frac{V}{A\,D} = \left(\frac{r_h}{R}\right)^2\left(\frac{H}{D}\right) \ll 1$);
- linear response of the resonators, no turbulence.

Under these hypotheses, the right-going simple wave is modeled by the following coupled system of PDE and ODE

$$\begin{cases} \dfrac{\partial u}{\partial t} + \dfrac{\partial}{\partial x}\left(a u + b\,\dfrac{u^2}{2}\right) = c\,\dfrac{\partial^{-1/2}}{\partial t^{-1/2}}\dfrac{\partial u}{\partial x} + d\,\dfrac{\partial^2 u}{\partial x^2} - e\,\dfrac{\partial p}{\partial t}, & \text{(4a)} \\ \dfrac{\partial^2 p}{\partial t^2} + f\,\dfrac{\partial^{3/2} p}{\partial t^{3/2}} + g\,p = h\,u, & \text{(4b)} \end{cases}$$

with the parameters

$$\begin{aligned} &a = a_0, \qquad b = \frac{\gamma+1}{2}, \qquad c = \frac{C\,a_0\sqrt{\nu}}{R^*}, \qquad d = \frac{\nu_d}{2}, \\ &e = \frac{V}{2\,\rho_0\,a_0\,A\,D}, \qquad f = \frac{2\,\sqrt{\nu}}{r}, \qquad g = \omega_0^2, \qquad h = \omega_0^2\,\frac{\gamma\,p_0}{a_0}. \end{aligned} \tag{5}$$

The PDE (4a) involves nonlinear advection (a and b) with losses due to viscous boundary layers in the tube (c) and to diffusivity of sound in the tube (d); see [5]. The ODE (4b) models the oscillation of Helmholtz resonators (g) with losses due to viscous boundary layers in the throat of resonators (f); see [22, 23]. The coupling between these equations is done by the coefficients e and h. If the resonators disappear ($H \to 0$ and thus $V \to 0$), then $e \to 0$: no coupling occurs, and one recovers the classical Chester's equation [20].

Fractional operators are involved in the system (4). In (4a), the Riemann-Liouville fractional integral of order 1/2 of a function $w(t)$ is defined by

$$\frac{\partial^{-1/2}}{\partial t^{-1/2}} w(t) = \frac{H(t)}{\sqrt{\pi\,t}} * w = \frac{1}{\sqrt{\pi}} \int_0^t (t-\tau)^{-1/2} w(\tau)\,d\tau, \tag{6}$$

where * is the convolution product in time with $H(t)$ the Heaviside function [19]. The fractional derivative of order 3/2 in (4b) is obtained by differentiating (6) twice with respect to t.

2.3. Dispersion analysis

In this section we present the dispersion analysis of (4), thus in the linear case $b = 0$. The obtained results will be useful to adjust the terms in the diffusive representation of the fractional derivatives (section 3.3).

Let us introduce the Fourier transforms in time and space

$$\widehat{w}(\omega) = \int_{-\infty}^{+\infty} w(t)\,e^{-i\,\omega\,t}\,dt, \qquad \widehat{w}(k) = \int_{-\infty}^{+\infty} w(x)\,e^{i\,k\,x}\,dx, \tag{7}$$

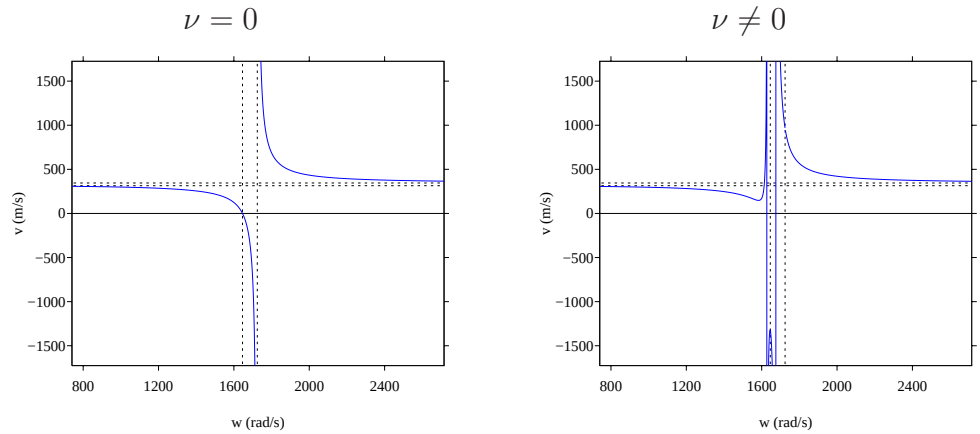

Figure 3: phase velocity in the linear regime, with resonators ($V \neq 0 \Leftrightarrow e \neq 0$). Inviscid ($\nu = 0$) and viscous ($\nu \neq 0$) case; see table 1 for the parameters. The vertical dotted lines denote ω_0 and ω_1. The horizontal dotted lines denote $\overline{v} < a_0$ and a_0 (12).

where ω is the angular frequency and k is the wavenumber. Applying these transforms to (4) provides a system of two linear equations whose determinant must be null, which yields the dispersion relation between ω and k. Defining the symbol of the half-order integral (6)

$$\chi(\omega) = \frac{1}{(i\,\omega)^{1/2}}, \tag{8}$$

and setting the coefficients

$$\begin{cases} \mathcal{D}_2(\omega) = i\,d[g - \omega^2(1 + f\,\chi)], \\ \mathcal{D}_1(\omega) = (a - c\,\chi)[g - \omega^2(1 + f\,\chi)], \\ \mathcal{D}_0(\omega) = \omega[\omega^2(1 + f\,\chi) - (g + e\,h)], \end{cases} \tag{9}$$

the dispersion relation takes the form

$$\mathcal{D}(k,\,\omega) = \mathcal{D}_2(\omega)\,k^2 + \mathcal{D}_1(\omega)\,k + \mathcal{D}_0(\omega) = 0. \tag{10}$$

Let us now describe this dispersion relation. First, we discuss the general case where the guide is coupled with resonators ($e \neq 0$). Neglecting the diffusivity of sound ($d = 0$), one obtains $k = -\mathcal{D}_0(\omega)\,/\,\mathcal{D}_1(\omega)$. Otherwise, (10) has two roots k_1 and k_2, and the root k with minimal modulus is selected.

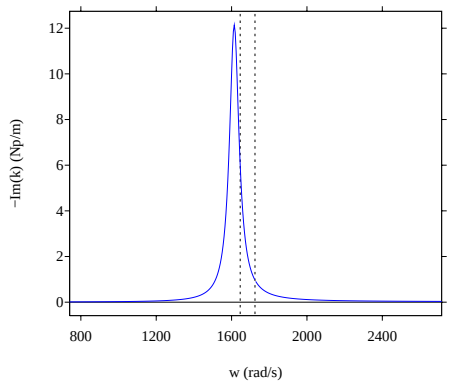

Figure 4: attenuation in the linear regime, with resonators ($V \neq 0 \Leftrightarrow e \neq 0$). Viscous case ($\nu \neq 0$); see table 1 for the parameters. The vertical dotted lines denote ω_0 and ω_1.

It follows the phase velocity $v = \omega \,/\, \Re\mathrm{e}(k)$ and the attenuation $-\Im\mathrm{m}(k)$. In the inviscid case ($c = f = 0$ adding to $d = 0$), one obtains the explicit expressions

$$v(\omega) = a_0 \frac{\omega^2 - \omega_0^2}{\omega^2 - \omega_1^2} \quad \text{and} \quad \Im\mathrm{m}(k) = 0, \tag{11}$$

where we have used (2) and (5). Basic properties of (11) are deduced:

$$\begin{cases} \overline{v} = v(0) = \dfrac{a_0}{1 + \dfrac{V}{2\,A\,D}} < a_0, \qquad v(\omega_0) = 0, \\ \lim\limits_{\omega \to \omega_1^{\pm}} v(\omega) = \mp\infty, \qquad \lim\limits_{\omega \to +\infty} v(\omega) = a_0, \\ v'(\omega) = -2\,a_0\,\omega_0^2 \left(\dfrac{V}{2\,A\,D}\right) \dfrac{\omega}{\left(\omega^2 - \omega_1^2\right)^2} < 0. \end{cases} \tag{12}$$

By assumption, $\frac{V}{A\,D} \ll 1$ and hence ω_1 is close to ω_0 (2). Far from ω_0 and ω_1, the curve of v is quite flat. In the viscous case ($c \neq 0$ and $f \neq 0$), the phase velocity does no more vanish at ω_0. Two vertical asymptotes of v occur near ω_0 and ω_1. When $\omega \to +\infty$, the horizontal asymptote of v is still a_0. On the other hand, the maximum of attenuation occurs near ω_0. These properties are illustrated in figures 3 and 4.

In the limit-case without resonators ($e = 0$), the linear dispersion relation (10) simplifies to

$$[g - \omega^2(1 + f\,\chi)][i\,d\,k^2 + k(a - c\,\chi) - \omega] = 0. \tag{13}$$

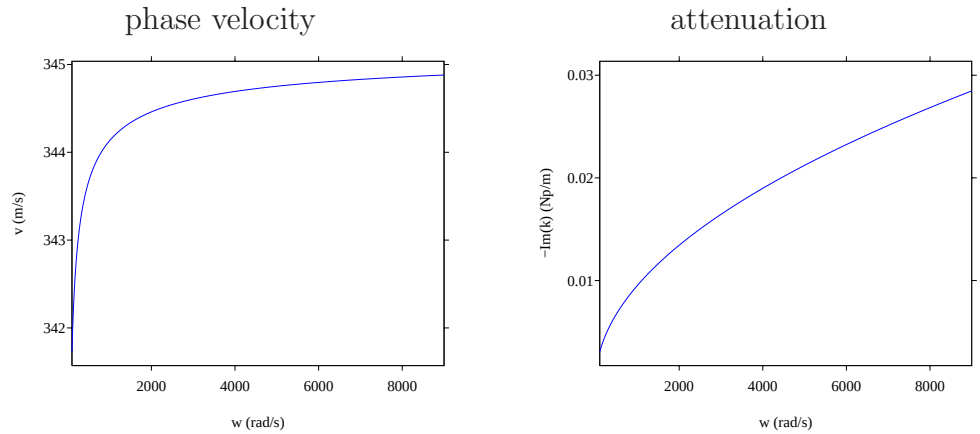

Figure 5: phase velocity and attenuation of the tube without resonators ($V = 0 \Leftrightarrow e = 0$). Viscous case ($\nu \neq 0$); see table 1 for the parameters.

In this product we focus on the part corresponding to (4b), i.e. the tube behavior, which leads to

$$i\,d\,k^2 + \left(a - \frac{c}{(i\,\omega)^{1/2}}\right) k - \omega = 0. \tag{14}$$

Neglecting the diffusivity of sound ($d = 0$) leads to the following phase velocity and the attenuation

$$\upsilon = \frac{a^2\,\omega - a\,c\sqrt{2\,\omega} + c^2}{a\,\omega - c\sqrt{\omega/2}}, \qquad \alpha = \frac{c}{\sqrt{2}}\,\frac{\omega^{3/2}}{a^2\,\omega - a\,c\,\sqrt{2\,\omega} + c^2}. \tag{15}$$

In the inviscid case ($c = d = 0$), the phase velocity is equal to a and the attenuation is null. Otherwise, one deduces the following properties:

$$\begin{cases} \upsilon(\omega) \underset{0}{\sim} -c\sqrt{\dfrac{2}{\omega}}, & \lim\limits_{\omega\to+\infty} \upsilon(\omega) = a_0, \\ \alpha(0) = 0, & \alpha(\omega) \underset{+\infty}{\sim} \dfrac{c}{a^2}\sqrt{\dfrac{\omega}{2}}, \end{cases} \tag{16}$$

radically different from the coupled case. These properties are illustrated in figure 5.

2.4. Regimes of propagation

An analysis of wave regimes has been performed in [29]. Under the hypothesis of weak nonlinearity, $\partial u/\partial x$ in (4a) is replaced by $-(1/a_0)\,\partial u/\partial t$ in the terms with coefficients b, c and d. The resulting system is written in the $(T,\, X)$ coordinates, where T is a non-dimensional retarded time, X is a non-dimensional slow space variable and ε is defined in (3):

$$T = \omega\left(t - \frac{x}{a_0}\right), \qquad X = \varepsilon\,\omega\,\frac{x}{a_0}. \tag{17}$$

The reduced variables $F = \mathcal{O}(1)$ and $G = \mathcal{O}(1)$ are introduced:

$$F = \frac{1}{\varepsilon}\,\frac{\gamma+1}{2}\,\frac{u}{a_0} = \frac{1}{\varepsilon}\,\frac{\gamma+1}{2\,\gamma}\,\frac{p^{'}}{p_0}, \qquad G = \frac{1}{\varepsilon}\,\frac{\gamma+1}{2\,\gamma}\,\frac{p}{p_0} = \frac{p}{p^{'}}\,F, \tag{18}$$

leading to

$$\begin{cases} \dfrac{\partial F}{\partial X} - F\,\dfrac{\partial F}{\partial T} = -\delta_R\,\dfrac{\partial^{1/2} F}{\partial T^{1/2}} + \beta\,\dfrac{\partial^2 F}{\partial T^2} - K\,\dfrac{\partial G}{\partial T}, & \text{(19a)} \\[2ex] \dfrac{\partial^2 G}{\partial T^2} + \delta_r\,\dfrac{\partial^{3/2} G}{\partial T^{3/2}} + \Omega\,G = \Omega\,F, & \text{(19b)} \end{cases}$$

with the new sets of parameters

$$\begin{aligned} &\delta_R = \frac{C}{\varepsilon\,R^*}\sqrt{\frac{\nu}{\omega}}, \qquad \beta = \frac{\nu_d\,\omega}{2\,\varepsilon\,a_0^2}, \qquad K = \frac{V}{2A\,D\,\varepsilon}, \\ &\delta_r = \frac{2}{r}\sqrt{\frac{\nu}{\omega}}, \qquad \Omega = \left(\frac{\omega_0}{\omega}\right)^2. \end{aligned} \tag{20}$$

The effect of dissipative terms δ_r, β and δ_R has been analyzed in [28, 29]; in particular, β is negligible. The dynamics of the system is mainly governed by the two parameters K and Ω. K is the ratio of geometrical dispersion terms with the nonlinearity effects. We assume that the resonators are coupled to the guide ($V \neq 0$), hence $\omega_0 \neq \infty$ and $0 < \Omega < +\infty$. Three limit-cases are then obtained in the inviscid case:

- first, if $K \ll 1$ or $\Omega \ll 1$, then one gets the evolution in a tube without resonators, leading to a shock

$$\frac{\partial F}{\partial X} - F\,\frac{\partial F}{\partial T} = 0; \tag{21}$$

- second, if $K \gg 1$, then (19) degenerates into a linear dispersive equation
$$\frac{\partial F}{\partial X} + K\,\frac{\partial F}{\partial T} + \frac{1}{\Omega}\frac{\partial^3 F}{\partial T^2 \partial X} = 0; \tag{22}$$
- third and last, if $\Omega \gg 1$, then one obtains the Korteweg-de Vries equation
$$\frac{\partial F}{\partial X} + K\,\frac{\partial F}{\partial T} - F\,\frac{\partial F}{\partial T} = \frac{K}{\Omega}\,\frac{\partial^3 F}{\partial T^3}. \tag{23}$$

This case is of particular interest, since it yields to solitons.

3. Mathematical modeling

3.1. Diffusive representation of fractional derivatives

Here we focus on the fractional terms in (4). The fractional integral (6) is non local in time, and relies on the full history of $w(t)$. A much more efficient formulation relies on a diffusive representation of this operator, which can be written equivalently [8]

$$\frac{\partial^{-1/2}}{\partial t^{-1/2}} w(t) = \int_0^{+\infty} \phi(\theta, t)\, d\theta, \tag{24}$$

where the diffusive variable ϕ defined by

$$\phi(\theta, t) = \frac{2}{\pi} \int_0^t e^{-(t-\tau)\,\theta^2} w(\tau)\, d\tau \tag{25}$$

satisfies the local-in-time differential equation

$$\begin{cases} \dfrac{\partial \phi}{\partial t} = -\theta^2\,\phi + \dfrac{2}{\pi}\,w, \\ \phi(\theta, 0) = 0. \end{cases} \tag{26}$$

To compute the derivative of order $3/2$, we start from the fractional integral (6) and derivate it twice. A first derivation leads to the derivative of order $1/2$:

$$\begin{aligned} \frac{\partial^{1/2}}{\partial t^{1/2}} w(t) &= \frac{d}{dt}\left(\frac{\partial^{-1/2}}{\partial t^{-1/2}} w(t)\right), \\ &= \frac{d}{dt}\left(\frac{1}{\sqrt{\pi}} \int_0^t (t-\tau)^{-1/2} w(\tau)\, d\tau\right), \\ &= \frac{1}{\sqrt{\pi}} \int_0^t (t-\tau)^{-1/2} w'(\tau)\, d\tau, \end{aligned} \tag{27}$$

where $w(0) = 0$ has been used. In the following of the paper $w(\cdot) = p(x, \cdot)$ and a zero initial condition $p(x, 0) = 0$ will always be chosen in the numerical tests. Then proceeding as previously for the fractional integral, a diffusive representation is introduced

$$\frac{\partial^{1/2}}{\partial t^{1/2}} w(t) = \int_0^{+\infty} \xi(\theta, t)\, d\theta, \tag{28}$$

where the diffusive variable ξ satisfies

$$\begin{cases} \dfrac{\partial \xi}{\partial t} = -\theta^2\, \xi + \dfrac{2}{\pi}\, w^{'}, \\ \xi(\theta, 0) = 0. \end{cases} \tag{29}$$

The derivative of order 3/2 is immediately deduced [6]:

$$\begin{aligned} \frac{\partial^{3/2}}{\partial t^{3/2}} w(t) &= \frac{d}{dt}\left(\frac{\partial^{1/2}}{\partial t^{1/2}} w(t) \right), \\ &= \int_0^{+\infty} \frac{\partial \xi}{\partial t}(\theta, t) d\theta, \\ &= \int_0^{+\infty} \left(-\theta^2\, \xi + \frac{2}{\pi}\, w^{'} \right) d\theta. \end{aligned} \tag{30}$$

Note that an alternative expression of the derivative of order 3/2 can also be obtained by derivating (27) which reads:

$$\frac{\partial^{3/2}}{\partial t^{3/2}} w(t) = \frac{1}{\sqrt{\pi}} \int_0^t (t - \tau)^{-1/2} w^{''}(\tau)\, d\tau,$$

if $w'(0) = 0$. Such an expression is less convenient than (30) since $w^{''}(\cdot) = \partial^2 p / \partial t^2 (x, \cdot)$ is involved but is not a natural unknown of the problem.

3.2. First-order system

To approximate the integral (24), a quadrature formula on N points is used, with weights μ_ℓ and abscissa θ_ℓ:

$$\frac{\partial^{-1/2}}{\partial t^{-1/2}} w(t) \simeq \sum_{\ell=1}^{N} \mu_\ell\, \phi(\theta_\ell, t) = \sum_{\ell=1}^{N} \mu_\ell\, \phi_\ell(t), \tag{31}$$

where the ϕ_ℓ satisfiy the ODE (26). Similarly, the integral (30) is written

$$\frac{\partial^{3/2}}{\partial t^{3/2}} w(t) \simeq \sum_{\ell=1}^{N} \mu_\ell \left(-\theta_\ell^2 \, \xi(\theta_\ell, t) + \frac{2}{\pi} \, w' \right) = \sum_{\ell=1}^{N} \mu_\ell \left(-\theta_\ell^2 \, \xi_\ell + \frac{2}{\pi} \, w' \right), \quad (32)$$

where the ξ_ℓ satisfy the ODE (29). The determination of weights and nodes μ_ℓ and θ_ℓ is discussed further. Then equations (4), (26, (29)), (31) and (32) are written as a first-order system

$$\begin{cases} \dfrac{\partial u}{\partial t} + \dfrac{\partial}{\partial x} \left(a u + b \, \dfrac{u^2}{2} \right) = c \displaystyle\sum_{\ell=1}^{N} \mu_\ell \phi_\ell + d \, \dfrac{\partial^2 u}{\partial x^2} - e \, q, \\ \dfrac{\partial p}{\partial t} = q, \\ \dfrac{\partial q}{\partial t} = h \, u - g \, p - f \displaystyle\sum_{\ell=1}^{N} \mu_\ell \left(-\theta_\ell^2 \, \xi_\ell + \dfrac{2}{\pi} \, q \right), \\ \dfrac{\partial \phi_\ell}{\partial t} - \dfrac{2}{\pi} \, \dfrac{\partial u}{\partial x} = -\theta_\ell^2 \, \phi_\ell, \qquad \ell = 1 \cdots N, \\ \dfrac{\partial \xi_\ell}{\partial t} = -\theta_\ell^2 \, \xi_\ell + \dfrac{2}{\pi} \, q, \qquad \ell = 1 \cdots N, \end{cases} \quad (33)$$

in an unbounded domain. The initial conditions are ($\ell = 1 \cdots N$)

$$\begin{aligned} & u(x,0) = u_0(x), \quad p(x,0) = p_0(x) \equiv 0, \quad \frac{\partial p}{\partial t}(x,0) = q_0(x) \equiv 0, \\ & \phi_\ell(x,0) = 0, \qquad \xi_\ell(x,0) = 0. \end{aligned} \quad (34)$$

Taking the vector of $(3 + 2\,N)$ unknowns

$$\mathbf{U} = (u, \, p, \, q, \phi_1, \cdots, \, \phi_N, \, \xi_1, \cdots, \, \xi_N)^T, \quad (35)$$

the system (33) can written in the form

$$\frac{\partial}{\partial t} \mathbf{U} + \frac{\partial}{\partial x} \mathcal{F}(\mathbf{U}) = \mathbf{S} \, \mathbf{U} + \mathbf{G} \, \frac{\partial^2}{\partial x^2} \mathbf{U}, \quad (36)$$

where $\mathcal{F}$ is the nonlinear flux function

$$\mathcal{F} = \left(a \, u + b \, \frac{u^2}{2}, \, 0, \, 0, \, -\frac{2}{\pi} u, \cdots, \, -\frac{2}{\pi} u, \, 0, \cdots, \, 0 \right)^T, \quad (37)$$

$\mathbf{G}$ is the $(3+2\,N)\times(3+2\,N)$ diagonal matrix $\mathrm{diag}(d,\,0,\cdots,\,0)$. $\mathbf{S}$ is the $(3+2\,N)\times(3+2\,N)$ diffusive matrix, in the sense that it contains the diffusive representation:

$$\mathbf{S}=\begin{pmatrix}
0 & 0 & -e & c\,\mu_1 & \cdots & c\,\mu_N & 0 & \cdots & 0\\
0 & 0 & 1 & 0 & \cdots & 0 & 0 & \cdots & 0\\
h & -g & -\dfrac{2}{\pi}f\displaystyle\sum_{\ell=1}^{N}\mu_\ell & 0 & \cdots & 0 & f\,\mu_1\,\theta_1^2 & \cdots & f\,\mu_N\,\theta_N^2\\
0 & 0 & 0 & -\theta_1^2 & & & & & \\
\vdots & \vdots & \vdots & & \ddots & & & & \\
0 & 0 & 0 & & & -\theta_N^2 & & & \\
0 & 0 & \dfrac{2}{\pi} & & & & -\theta_1^2 & & \\
\vdots & \vdots & \vdots & & & & & \ddots & \\
0 & 0 & \dfrac{2}{\pi} & & & & & & -\theta_N^2
\end{pmatrix}. \tag{38}$$

Three properties are deduced from (36):

- the eigenvalues of the Jacobian matrix $\mathbf{J}=\mathcal{F}'$ in (37) are real: $a+b\,u$, and 0 with multiplicity $2\,N+2$. These eigenvalues do not depend on the coefficients of the diffusive representation;
- if $N=0$, the eigenvalues of $\mathbf{S}$ are 0 and $\pm i\,\omega_1$, with $\omega_1=\sqrt{e\,h+g}$; see (2) and (5). If $N\neq 0$, the eigenvalues of $\mathbf{S}$ are not known, but numerical investigations indicate that the eigenvalues are close to 0, $-\varsigma\pm i\,\omega_1$ (with $0<\varsigma\ll 1$), and $-\theta_\ell^2$ with multiplicity 2 ($\ell=1,\cdots,N$);
- a linear dispersion analysis can be performed as in the original model (4). The formula (10) with coefficients (9) still holds, replacing χ in (8) by

$$\tilde{\chi}(\omega)=\frac{2}{\pi}\sum_{\ell=1}^{N}\frac{\mu_\ell}{\theta_\ell^2+i\,\omega}. \tag{39}$$

3.3. Coefficients of the diffusive representation

It remains to determine the $2\,N$ coefficients of the diffusive representation μ_ℓ and θ_ℓ in (38), issued from (31) and (32). This issue is crucial both for the

accuracy of the modeling and for the computational efficiency of the method. Two strategies exist for this purpose.

The first one relies on Gaussian quadratures of improper integrals (24) and (30). A Laguerre quadrature formula can be used for this purpose [9]. This technique is frequently used in the literature [35, 18, 8, 1], ensuring positive weights and nodes; a short discussion on that topic is proposed in section 6. Moreover, Laguerre quadrature does not depend on the frequency content of the waves, which may be advantageous in nonlinear problems, where harmonics are generated. However despite these advantages we have tried this approach and it gives very poor results. As shown further, a large number of memory variables is required to get acceptable accuracy, which greatly increases the computational cost.

Here we propose a much more efficient strategy, based on the dispersion relation (10). The original problem (4) and the first-order system (36) differ only in their symbol $\chi(\omega)$: (8) in the first case, (39) in the second one. Adjusting them provides a way to estimate μ_ℓ and θ_ℓ. This technique is physically meaningful, and has proven its efficiency in a previous work about poroelastic waves [2]. Let $Q(\omega)$ be the optimized quantity and Q_{ref} the desired one:

$$\begin{aligned} Q(\omega) &= \frac{\tilde{\chi}(\omega)}{\chi(\omega)} = \frac{2}{\pi} \sum_{\ell=1}^{N} \frac{\mu_\ell}{\theta_\ell^2 + i\,\omega} \left(i\,\omega\right)^{1/2} = \sum_{\ell=1}^{N} \mu_\ell\, q_\ell(\omega), \\ Q_{ref}(\omega) &= 1. \end{aligned} \tag{40}$$

We implement a linear optimization procedure [12, 2] in order to minimize the distance between Q and Q_{ref} in the interval $[\omega_{min}, \omega_{max}]$ containing the characteristic angular frequency ω of the initial pulse. The abscissas θ_ℓ are chosen distributed linearly on a logarithmic scale

$$\theta_\ell^2 = \omega_{min} \left(\frac{\omega_{max}}{\omega_{min}}\right)^{\frac{\ell-1}{N-1}}, \qquad \ell = 1, ..., N. \tag{41}$$

The weights μ_ℓ are obtained by solving the system

$$\sum_{\ell=1}^{N} \mu_\ell\, q_\ell(\tilde{\omega}_k) = 1, \qquad k = 1, ..., K, \tag{42}$$

where the $\tilde{\omega}_k$ are also distributed linearly on a logarithmic scale of K points

$$\tilde{\omega}_k = \omega_{min} \left(\frac{\omega_{max}}{\omega_{min}} \right)^{\frac{k-1}{K-1}}, \qquad k = 1, ..., K. \tag{43}$$

Since the $q_\ell(\omega)$ are complex functions, optimization is performed simultaneously on the real and imaginary parts

$$\begin{cases} \sum_{\ell=1}^{N} \mu_\ell \, \mathbb{R}\mathrm{e}(q_\ell(\tilde{\omega}_k)) & = 1, \\ \sum_{\ell=1}^{N} \mu_\ell \, \mathbb{I}\mathrm{m}(q_\ell(\tilde{\omega}_k)) & = 0, \qquad k = 1, ..., K. \end{cases} \tag{44}$$

A square system is obtained when $2K = N$, whereas $2\,K > N$ yields an overdetermined system, which can be solved by writing normal equations [9]. The quality of resolution deteriorates as N increases or as the interval $[\omega_{min}, \omega_{max}]$ decreases. In the numerical experiments, we use even values of N and $2K = N$. The interval of optimisation $[\omega_{min}, \omega_{max}]$ depends on the configuration under study:

- for the coupled system with resonators, the attenuation is bounded (figure 4), and the existence of smooth solitary waves maintains globally the frequency content of the initial disturbance. Consequently, we choose a narrow interval centered around ω, by taking for instance $\omega_{min} = \omega \,/\, 2$ and $\omega_{max} = \omega \times 3/2$;

- for the tube without resonators, shocks are expected. Consequently, higher harmonics are generated, and we propose to use $\omega_{min} = \omega \,/\, 2$ but $\omega_{max} = \omega \times \mathcal{N}$, where $\mathcal{N}$ is the number of harmonics of interest in a Fourier decomposition of the wave [20]. In numerical experiments, we take $\mathcal{N} = 20$.

Figure 6 illustrates how the number of diffusive variables influences the accuracy of the optimisation procedure, in the case of the coupled system. In the left part, we show the error $|Q(\omega) - 1|$ for various values of N. The vertical dotted lines represent the range of optimisation. By construction, the error vanishes at the abscissae $\tilde{\omega}_k$. As expected, the accuracy of the diffusive approximation increases with N. The right part of the figure displays the error of model $\varepsilon_m = ||Q(\omega) - 1||_{L_2}$ on the range of interest, in terms of N

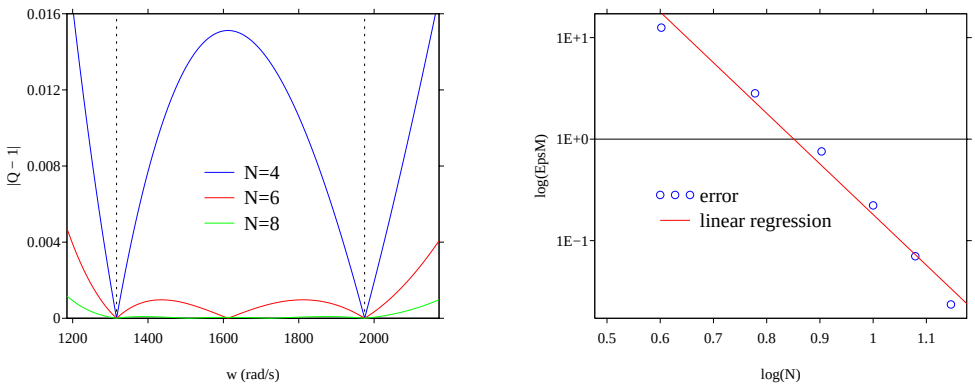

Figure 6: error of model due to the optimisation procedure, for the coupled system (tube with resonators, $V \neq 0$). Left: $|Q(\omega)-1|$ in (40), for various numbers of diffusive variables N; the vertical dotted lines denote the upper and lower ranges of optimisation ω_{min} and ω_{max}. Right: $\varepsilon_m = ||Q(\omega)-1||_{L_2}$, in terms of N; the slope of the linear regression is -5.

and in log-log scale. The measured values are close to a straight line with slope -5, hence one can postulate a power-law $\varepsilon_m \approx \varepsilon_0(1/N)^5$.

The role of diffusive representation on linear attenuation is illustrated in figure 7. The attenuation of the exact model (4) is compared to the approximate diffusive model (36). The top of the figure concerns the coupled system. When Laguerre quadrature is used, the resonance peak is shifted and poor accuracy is obtained even with $N = 50$, involving 103 unknowns in (35). On the contrary, $N = 6$ is sufficient to get excellent agreement if optimisation is used, involving only 15 unknowns in (35). The bottom of the figure concerns the guide without Helmholtz resonators. Similar accuracy is obtained with $N = 50$ if Laguerre is used, and with $N = 12$ if optimisation is used.

4. Numerical modeling

4.1. Splitting

In order to integrate the system (36), a grid is introduced, with a uniform spatial mesh size Δx and a variable time step Δt_n, which for the sake of simplicity will be noted Δt. The approximation of the exact solution $\mathbf{U}(x_j = j\,\Delta\,x, t_n = t_{n-1} + \Delta t)$ is denoted by $\mathbf{U}_j^n$. Unsplit integration of (36) is not optimal, because the time step stability condition involves the spectral radius

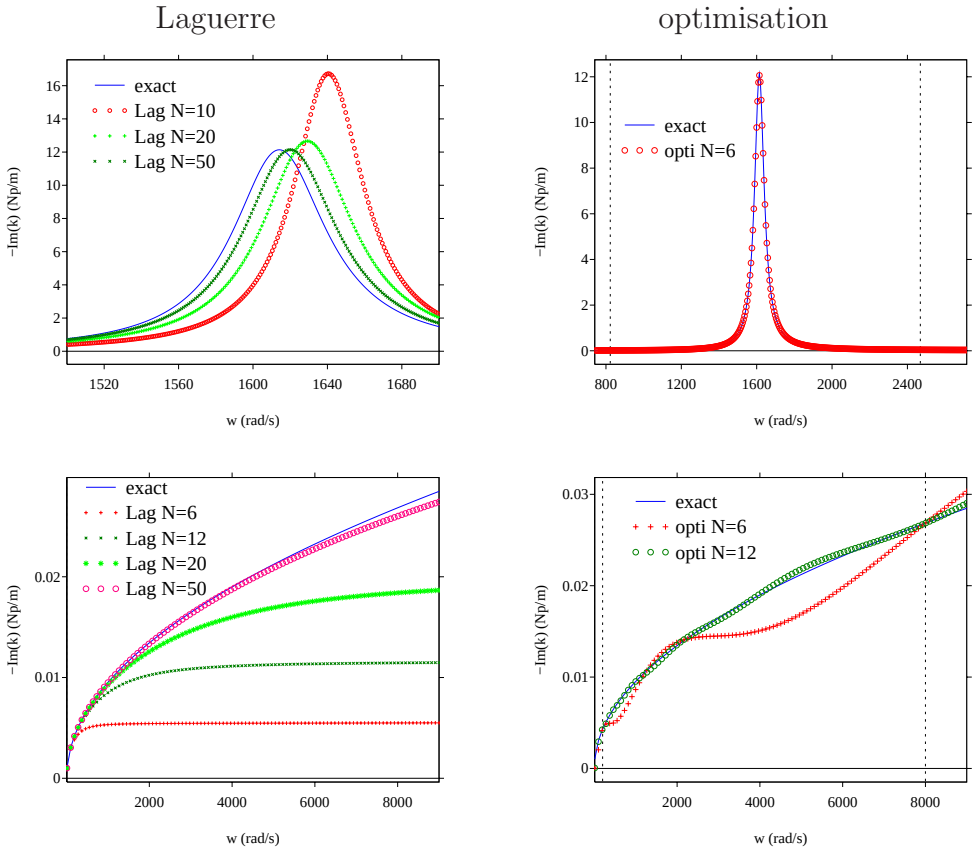

Figure 7: attenuation in the viscous linear regime. Comparison between the exact fractional model (4) and the approximate diffusive model (36). Left: Laguerre quadrature; right: optimisation. Top: coupled system with resonators; bottom: tube without resonators. The vertical dotted lines denote the range of optimisation $[\omega_{min}, \omega_{max}]$.

of $\mathbf{S}$ which grows in an unbounded way with N. Moreover, it requires to build an adequate scheme for the coupled system.

A more efficient strategy is adopted here, which consists in splitting the original system (36) into a propagative part (45a) and a diffusive part (45b)

$$\begin{cases} \dfrac{\partial}{\partial t}\mathbf{U} + \dfrac{\partial}{\partial x}\mathcal{F}(\mathbf{U}) = \mathbf{G}\,\dfrac{\partial^2}{\partial x^2}\mathbf{U}, & \text{(45a)} \\ \dfrac{\partial}{\partial t}\mathbf{U} = \mathbf{S}\,\mathbf{U}. & \text{(45b)} \end{cases}$$

The discrete operators associated with steps (45a) and (45b) are denoted by $\mathbf{H}_a$ and $\mathbf{H}_b$, respectively. The second-order Strang splitting [15, 14] is then used between t_n and t_{n+1}, giving the time-marching

$$\begin{aligned} \bullet\ \mathbf{U}_j^{(1)} &= \mathbf{H}_b(\tfrac{\Delta t}{2})\,\mathbf{U}_j^n, \\ \bullet\ \mathbf{U}_j^{(2)} &= \mathbf{H}_a(\Delta t)\,\mathbf{U}_j^{(1)}, \\ \bullet\ \mathbf{U}_j^{n+1} &= \mathbf{H}_b(\tfrac{\Delta t}{2})\,\mathbf{U}_j^{(2)}. \end{aligned} \tag{46}$$

4.2. Propagative part

The propagative part (45a) is solved by any standard scheme for nonlinear hyperbolic PDE:

$$\begin{aligned} u_j^{n+1} &= u_j^n - \frac{\Delta t}{\Delta x}\left(\mathcal{F}^1_{j+1/2} - \mathcal{F}^1_{j-1/2}\right) + \frac{d\,\Delta t}{\Delta x^2}\left(u_{j+1}^n - 2\,u_j^n + u_{j-1}^n\right), \\ \phi_{j,\ell}^{n+1} &= \phi_{j,\ell}^n + \frac{1}{\pi}\frac{\Delta t}{\Delta x}\left(u_{j+1}^n - u_{j-1}^n\right), \qquad \ell = 1, \cdots, N, \end{aligned} \tag{47}$$

where $\mathcal{F}^1_{j\pm1/2}$ is the numerical flux function of the advection-Burgers part in (37). In practice, a second-order TVD scheme with MC-limiter is used in our numerical experiments [15]. Stability analysis of (47) provides the necessary and sufficient condition [27, 7]

$$\frac{\alpha^2 - \alpha}{2} \le \delta \le \frac{1-\alpha}{2}, \tag{48}$$

with the adimensionalized parameters α and δ and the discrete velocity $a^{(n)}_{\max}$

$$\alpha = a^{(n)}_{\max}\frac{\Delta t}{\Delta x}, \qquad \delta = d\frac{\Delta t}{\Delta x^2}, \qquad a^{(n)}_{\max} = a + b\,\max_j(u_j^n). \tag{49}$$

The condition (48) is proven rigorously in the case of the advection equation and the upwind scheme, but numerical experiments indicate that it still holds for the nonlinear advection (modifying a into $a_{\max}^{(n)}$) and for the TVD scheme. Solving (48)-(49) gives the condition

$$\alpha \leq \min\left(1+\frac{1}{\mathrm{Pe}}, \frac{1}{1+\frac{1}{\mathrm{Pe}}}\right), \tag{50}$$

where $\mathrm{Pe} = \alpha/2\delta = a_{\max}^{(n)}\,\Delta x/2\,d$ is the discrete Péclet number. In our configuration, $\mathrm{Pe} \approx 10^5$ which leads to the restriction on the time step

$$\frac{a_{\max}^{(n)}\Delta t}{\Delta x} \leq \left(1+\frac{1}{\mathrm{Pe}}\right)^{-1} \approx 1-\frac{1}{\mathrm{Pe}} \approx 1. \tag{51}$$

Therefore despite the explicit discretization of $d\,\partial^2 u/\partial x^2$, the optimal CFL condition is maintained.

4.3. Diffusive part

Since the physical parameters do not vary with time, the diffusive part (45b) can be solved exactly. This gives

$$\mathbf{H}_b\left(\frac{\Delta\, t}{2}\right)\,\mathbf{U}_j = e^{\mathbf{S}\frac{\Delta\, t}{2}}\,\mathbf{U}_j. \tag{52}$$

In the inviscid case $\nu = 0$, only the unknowns p, q and u are involved, and since $N = 0$, the exponential can be computed analytically. Using ω_1 (2) and defining $\tau = \Delta t/2$, one obtains:

$$e^{\mathbf{S}\tau} = \begin{pmatrix} \frac{1}{\omega_1^2}\left(g + e\,h\,\cos\omega_1\tau\right) & \frac{e\,g}{\omega_1^2}\left(1-\cos\omega_1\tau\right) & -\frac{e}{\omega_1}\sin\omega_1\tau \\ \frac{h}{\omega_1^2}\left(1-\cos\omega_1\tau\right) & \frac{1}{\omega_1^2}\left(e\,h + g\,\cos\omega_1\tau\right) & \frac{1}{\omega_1}\sin\omega_1\tau \\ \frac{h}{\omega_1}\sin\omega_1\tau & -\frac{g}{\omega_1}\sin\omega_1\tau & \cos\omega_1\tau \end{pmatrix}. \tag{53}$$

In the general case $N > 0$, it is computed numerically using a $(6,6)$ Padé approximation in the "scaling and squaring method" [21]. If the physical parameters are constant, the computation is done only once at each time

step, leading to a negligible computational cost. Even in the case $N = 0$, it is twice faster to use the numerical evaluation of $e^{\mathbf{S}\tau}$ than computing (53), because of the numerical evaluations of trigonometric functions.

This part of the splitting is unconditionally stable, so that the global stability requirement is (51) and is not penalized by the diffusive part. In other words, the time step only depends on the advection and on the Burgers coefficient in (4). In particular, Δt does not depend on the fractional parameters c and f or on the coupling parameters e and h.

5. Numerical experiments

5.1. Configuration

γ	p_0 (Pa)	ρ_0 (kg/m^3)	Pr	ν (m^2/s)	μ_v/μ
1.403	10^5	1.177	0.708	$1.57\,10^{-5}$	0.60
R (m)	D (m)	r (m)	L (m)	r_h (m)	H (m)
0.04	0.05	0.00355	0.0356	0.0125	0.1

Table 1: physical parameters of air at 15 °C, and geometrical data from [32].

The physical and geometrical parameters are given in table 1. The physical data correspond to air at 15 °C, and the geometrical data are issued from [32]. From (2), one obtains $a_0 = 345.25$ m/s, $C = 1.478$ and $\nu_d = 3.92\,10^{-5}$ m^2/s. One deduces the parameters of the PDE (4)-(5), given in the upper part of table 2. The tube of length $\mathcal{L} = 80$ m is discretized on $N_x = 8000$ grid nodes. The maximal CFL number is $1 - 1/\mathrm{Pe}$, where the Péclet number is $\mathrm{Pe} = 1.75\,10^5$ (51); in practice, we take the CFL number equal to 0.95. Lastly, a set of 10 receivers is put on the computational domain at abscissas $x_r = 15 + 5\,(i-1)$, $i = 1 \cdots 10$, where the time history of u is recorded at each time step.

Except in section 5.3, computations are initialized by a Gaussian pulse or by a door pulse on the velocity

$$u_0(x) = \begin{cases} u_m \exp\left(-\left(\dfrac{x - x_0}{\sigma}\right)^2\right), \\ u_m \left(\mathcal{H}\left(x - x_0 - \dfrac{\lambda}{2}\right) - \mathcal{H}\left(x - x_0 + \dfrac{\lambda}{2}\right)\right), \end{cases} \tag{54}$$

where $\mathcal{H}$ is the Heaviside function and $x_0 = 7$ m. λ is the width of the door pulse, and is also the width of the Gaussian pulse: taking $\sigma = \lambda/2\sqrt{\ln 100}$

a (m/s)	345.25
b	1.20
c (m/s$^{3/2}$)	50.42
d (m^2/s)	$1.96\,10^{-5}$
e (m/s^3/Pa)	$2.40\,10^{-4}$
f (s$^{-1/2}$)	2.23
g (s^2)	$2.70\,10^{6}$
h (Pa/m/s)	$1.10\,10^{9}$
ω_0 (rad/s)	1645.67
ω_1 (rad/s)	1724.16
$\overline{v}$ (m/s)	314.53

Table 2: coefficients of the PDE (4). Lower part: natural angular frequencies (2), and low frequency limit of the phase velocity (11) in the coupled system.

gives $u_0(x) = u_m/100$ at $x = x_0 \pm \lambda/2$. All the other initial conditions in (34) are null.

The key parameters governing the evolution of the system are K and Ω (20); see section 2.4. On one hand, we take $K = 0.5$ which ensures a nonlinear regime of propagation. It follows the amplitude $u_m \approx 56.12$ m/s (54), the parameter of nonlinearity $\varepsilon = 0.19$, the overpressure $p^{'}/p_0 = 0.22$ and the sound intensity $I = 181.1$ dB (3). On the other hand, we take $\Omega = 1$ or $\Omega = 16$, yielding theoretically to dispersive waves and solitons, respectively. In the case $\Omega = 1$, the linear dispersion analysis predicts a maximal attenuation. In the case $\Omega = 16$, the natural frequency is $\omega = 411.4$ rad/s and the central wavelength is $\lambda = 5.27$ m.

5.2. Test 1: nonlinear acoustics

In a first test, the height of the cavity is $H = 0$, hence $e = 0$ and no coupling occurs with the Helmholtz resonators. The dispersion relation is therefore (14), and the key adimentionalized parameters of section 2.4 are $K = 0$ and $\Omega = +\infty$. The number of diffusive variables is $N = 12$; since no memory variables ξ are required to model dissipative effects in the resonators, only 15 variables are involved in (35). Optimisation of the coefficients μ_ℓ is performed between $\omega_{min} = 185$ rad/s and $\omega_{max} = 8228$ rad/s (section 3.3).

In the inviscid case, where only the coefficients a and b are non-null in (4), smooth initial data develop shocks in finite time, yielding a decrease of

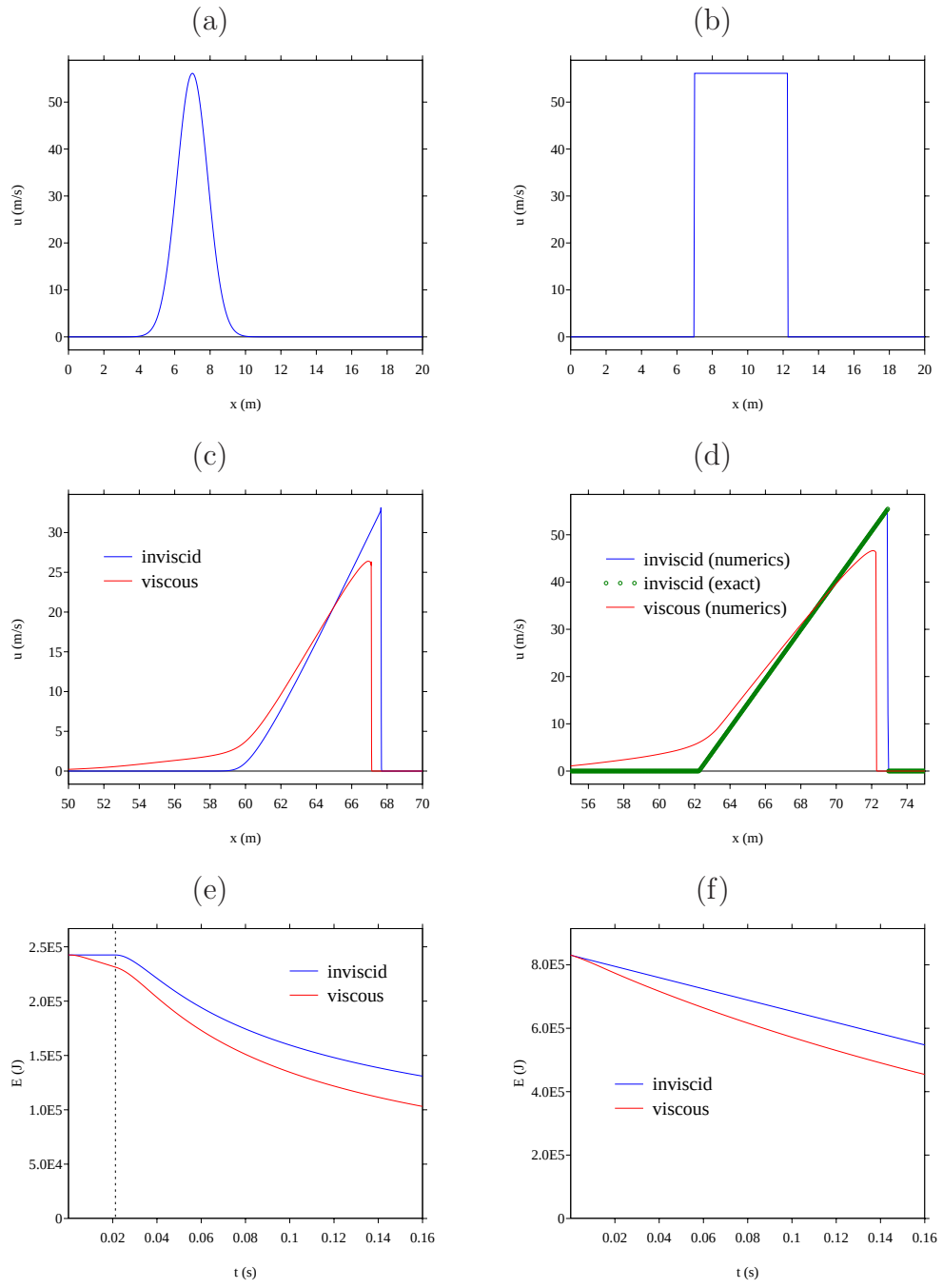

Figure 8: test 1. Nonlinear acoustics without oscillators, for a Gaussian pulse (left row) and a door pulse (right row). (a-b): initial pulse. (c-d): numerical and exact solution at $t = 0.16$ s. (e-f): time evolution of the energy; in (e), the vertical dotted line denote the time of shock t^*.

energy. The Gaussian initial pulse breaks at time

$$t^* = \sqrt{\frac{e}{2}} \frac{\sigma}{u_m\, b}, \tag{55}$$

where the Neper constant $e \approx 2.71$ must not be confused with the null coefficient in (4a). It gives the time break $t^* = 0.021$ s (55).

Figure 8 shows the initial values of the solution at the initial instant (a-b) and at $t = 0.16$ s $> t^*$ (c-d), which corresponds roughly to 7000 time steps. Both the inviscid case and the viscous case are displayed, where the viscous boundary layer in the tube and the diffusivity of sound are accounted for. In the inviscid case, typical nonlinear phenomena are observed: shock on the right part of the Gaussian pulse (c), rarefaction waves and right-going shock for the door pulse (d). In this latter case, good agreement is obtained with the exact solution. In the viscous case, these phenomena are qualitatively maintained. A small decrease of amplitude is observed, together with a tail on the left part of the waves. The key issue is that viscous effects are not sufficient to prevent from the occurrence of a shock (c) or to smooth an existing discontinuity (d), which confirms the theoretical analysis performed in [28].

Lastly, time evolution of the energy $E^{(n)} = \sum_j (u_j^n)^2$ is displayed in (e-f). For the Gaussian pulse in the inviscid case (e), energy is conserved as long as the wave is smooth; at the scale of the figure, numerical diffusion is not seen. From $t = t^*$ where the shock appears, energy decreases. For the door pulse in the inviscid case (e), energy decreases linearly with time. The results are qualitatively the same in the viscous cases, with a greater decrease of energy.

5.3. Test 2: fractional oscillations in Helmholtz resonators

As a second validation test, we focus on the fractional oscillator of order 3/2. The coupling with nonlinear acoustics in the tube is neglected, and we solve (4b) with no coupling $h = 0$. The initial value of pressure is $p_0(x) = 1$ and $p_1(x) = 0$, leading to oscillations with damping. The analytical solution is obtained in terms of fractional power series on 200 modes: see equation (10) of [6]. The numerical solution is obtained by solving the following problem

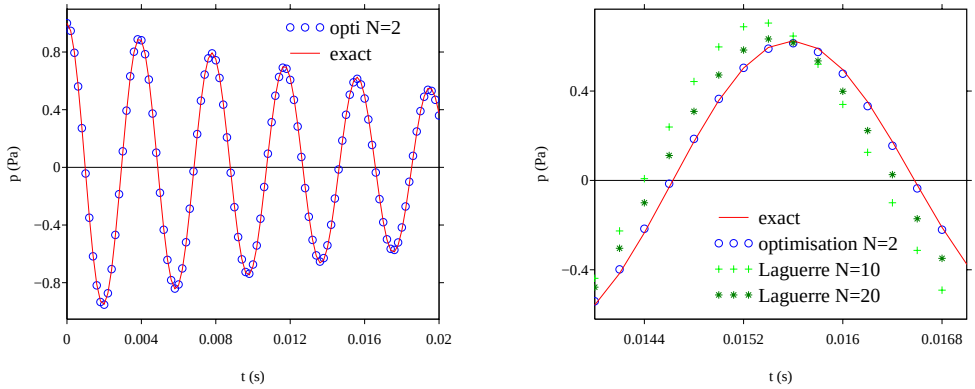

Figure 9: test2. Fractional oscillator of order 3/2. Comparisons between the numerical solution and the exact solution (right row: zoom).

with $N+2$ unknows

$$\left\{\begin{array}{l} \dfrac{\partial p}{\partial t} = q, \\ \dfrac{\partial q}{\partial t} = -g\,p - f\,\displaystyle\sum_{\ell=1}^{N} \mu_\ell \left(-\theta_\ell^2\,\xi_\ell + \frac{2}{\pi}\,q\right), \\ \dfrac{\partial \xi_\ell}{\partial t} = -\theta_\ell^2\,\xi_\ell + \dfrac{2}{\pi}\,q, \qquad\qquad \ell = 1 \cdots N. \end{array}\right. \tag{56}$$

Therefore the numerical solution is the exact solution of the system (52) with N memory variables; consequently, the only error is the error of model ε_m, due to the quadrature of the diffusive representation.

Figure 9 shows the influence of the quadrature rule on the accuracy of the modeling. When optimisation is used, only $N = 2$ memory variables are required to obtain an excellent agreement with exact solution (left row). On the contrary, large errors are observed when Laguerre quadrature is used, even with $N = 20$.

5.4. Test 3: linear dispersive waves

In a third test, we consider the coupled system with resonators, in the linear regime: $b = 0$ in (4). The simulations are initialized by a Gaussian pulse, and they are performed during 8000 time steps. The computations are done with and without the viscous effects of boundary layers and diffusivity of sound. The number of diffusive variables is $N = 6$, involving 15 variables

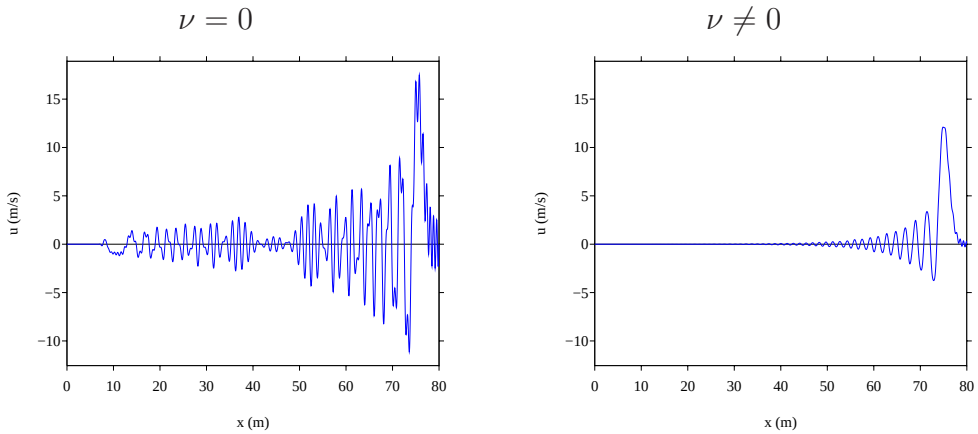

Figure 10: test3. Linear coupled system, with a Gaussian pulse and $\Omega = 1$. Snapshots of u after 8000 time steps. Left: invicid case; right: viscous case.

in (35). Optimisation of the diffusive coefficients μ_ℓ is performed between $\omega_{min} = 822$ rad/s and $\omega_{max} = 2468$ rad/s if $\Omega = 1$, and values 4 times smaller if $\Omega = 16$ (section 3.3).

The case $\Omega = 1$ is shown in figure 10. High dispersion is observed in the inviscid case, which confirms the dispersion analysis performed in section 2.3 (see figure 3, near the vertical dotted lines). The oscillations are highly damped in the viscous case, due to the large value of attenuation (see figure 4).

The case $\Omega = 16$ is displayed in figure 11. Compared with figure 10, the dispersion is greatly reduced. In the inviscid case, an oscillating mode remains at the place of initialization; moreover, the energy is conserved (not shown here). The static mode is damped in the viscous case. Seismograms are built from the time signals stored at the receivers. Then, the celerity $\mathcal{V}$ of the highest amplitude is numerically measured. One obtains $\mathcal{V} = 312.02$ m/s (if $\nu = 0$) and $\mathcal{V} = 310.39$ m/s (if $\nu \neq 0$). These values are close to the zero-frequency limit $\overline{v} = 314.53$. The slight difference is due to the large-band of the intial pulse.

5.5. Test 4: acoustic solitary waves

Lastly, we consider the full coupled system in the nonlinear regime. Computations are initialized by a Gaussian pulse, and simulations are performed during 8000 time steps, which corresponds roughly to 0.20 s of propagation. The case $K = 0.5$ and $\Omega = 1$ is shown in figure 12, to be compared with

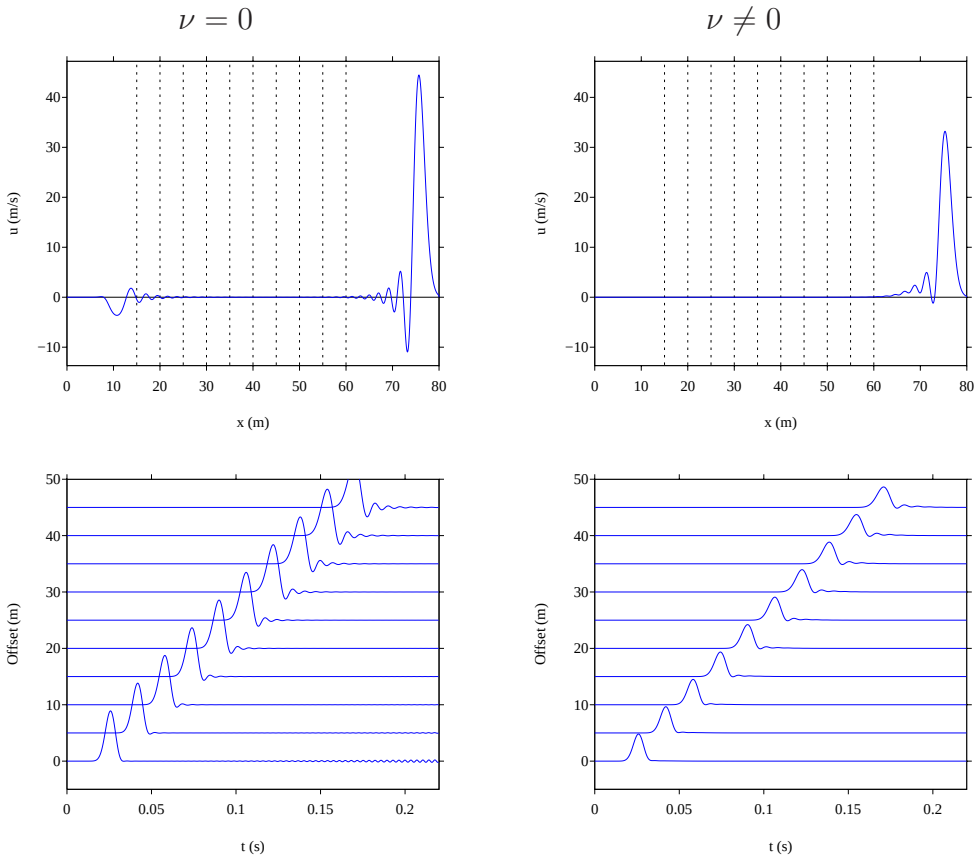

Figure 11: test3. Linear coupled system, with a Gaussian pulse and $\Omega = 16$. Left: invicid case; right: viscous case. Top: snapshot of u after 8000 time steps (the vertical dotted lines denote the receivers); bottom: seismograms.

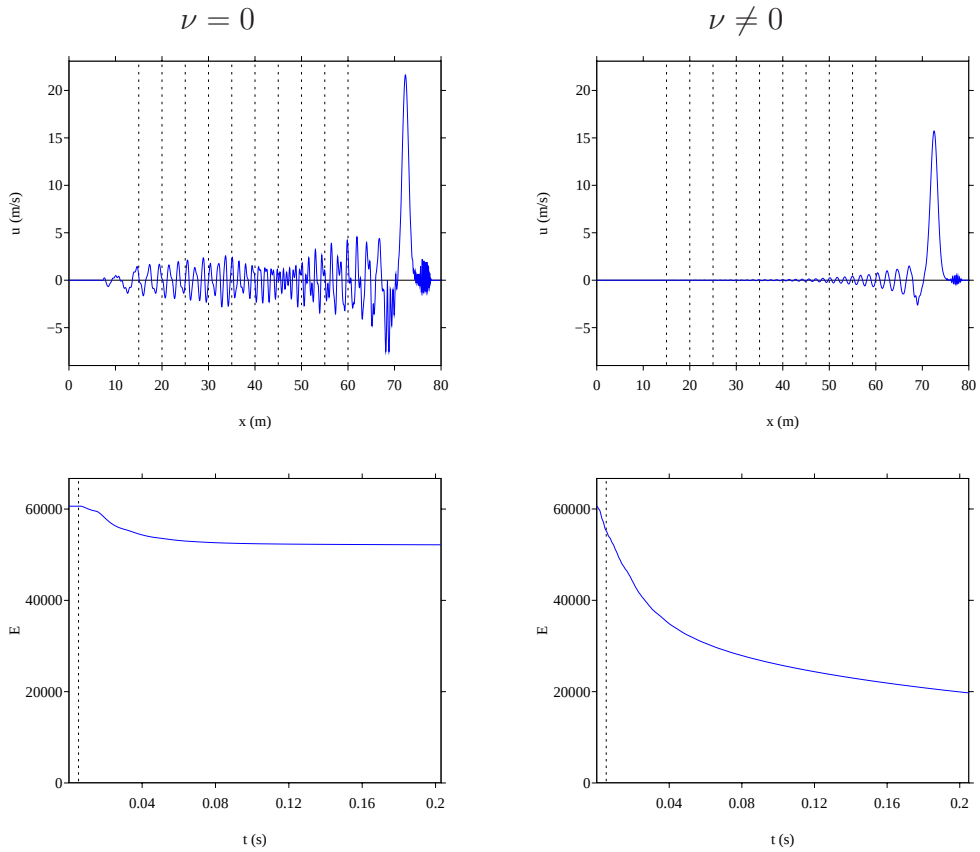

Figure 12: test4. Nonlinear coupled system, with a Gaussian pulse, $K = 0.5$ and $\Omega = 1$. Left: viscous case; right: inviscid case. Top: snapshots of u after 8000 time steps (the vertical dotted lines denote the receivers); bottom: time evolution of the energy (the vertical dotted line denotes t^* (55).

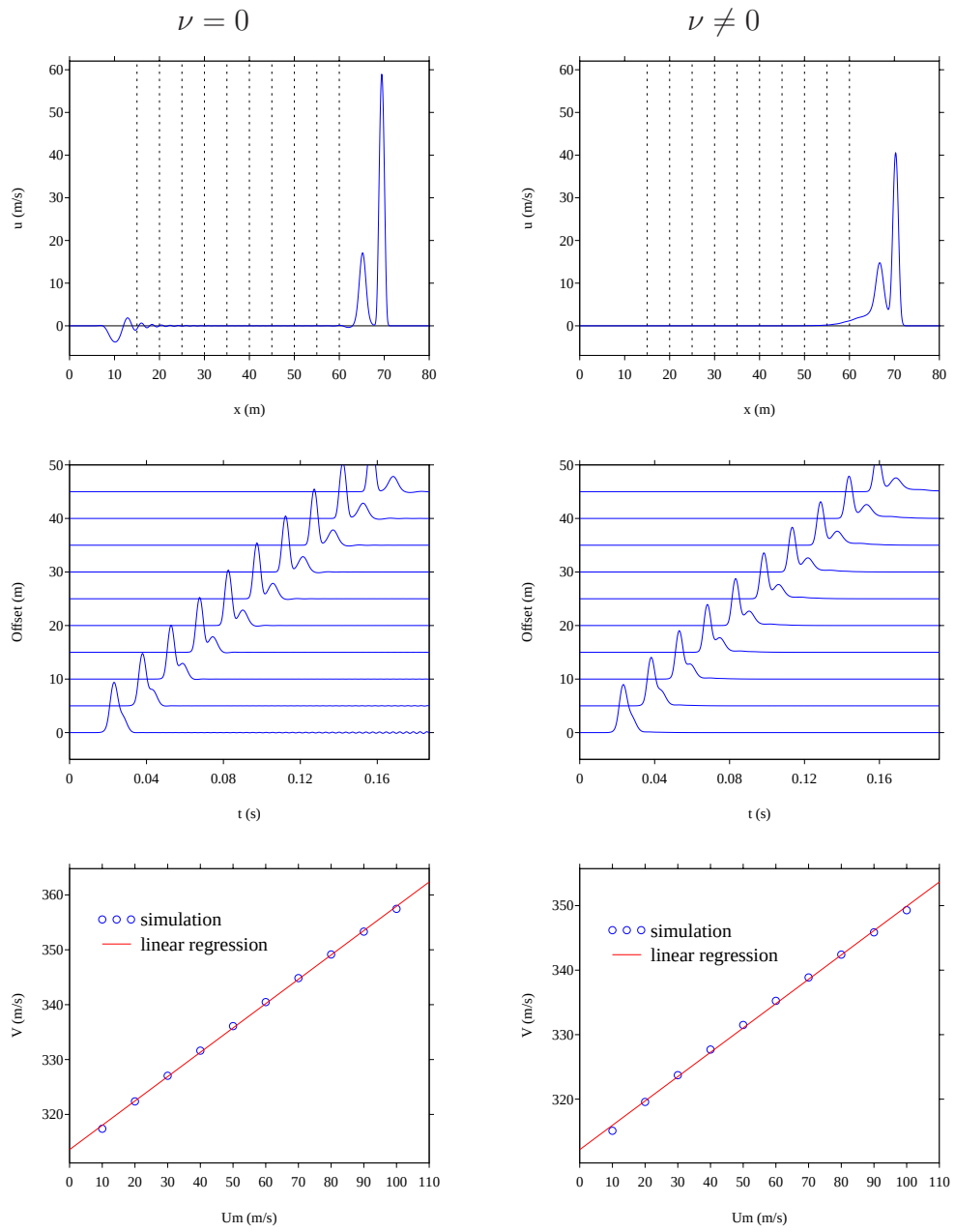

Figure 13: test4. Nonlinear coupled system, with a Gaussian pulse, $K = 0.5$ and $\Omega = 16$. Top: snapshot of u after 8000 time steps. Middle: seismograms. Bottom: celerity $\mathcal{V}$ vs amplitude u_m (from 10 m/s to 100 m/s).

the figure 10 obtained in the linear regime. A ballistic signal is observed, followed by a highly dispersive coda: no solitary wave emerges. If $\nu \neq 0$, a large amount of attenuation is also introduced, that damps this coda. In the inviscid case, the energy begins to decrease and then is almost conserved. It means that the initial smooth pulse has lead to a shock, and then an equilibrium with dispersion has lead to the emergence of a smooth structure. Similar conclusion is reached in the viscous case, except that energy always decreases.

The case $K = 0.5$ and $\Omega = 16$ is displayed in figure 13, to be compared with figure 11 obtained in the linear regime. We recall that the theoretical analysis predicts the existence of solitary waves (section 2.4). Compared with figure 12, the coda has disappeared. In the inviscid case, an oscillating mode remains at the place of initialization; moreover, the energy is conserved (not shown here), which indicates that no shock has been created. Two smooth structures are observed. Longer simulations show that these two components separate and propagate at different speeds. In the sequel, we examine whether these solitary waves have the classical properties of solitons.

In the case $K = 0.5$ and $\Omega = 16$, seismograms are built from the time signals stored at the receivers. One measures numerically the celerity $\mathcal{V}$ of the nonlinear wave with highest amplitude. Similar measures are done for various amplitudes u_m of the incident pulse, from 10 m/s to 100 m/s, or equivalently from $K = 2.80$ to $K = 0.28$. It is observed that $\mathcal{V}$ increases linearly with u_m: a linear regression estimation yields $\mathcal{V} = 313.58 + 0.4435\, u_m$ (if $\nu = 0$) and $\mathcal{V} = 312.17 + 0.3773\, u_m$ (if $\nu \neq 0$). Waves propagate slightly faster in the inviscid case, because attenuation decreases the amplitude and consequently the celerity. The limit for $u_m = 0$ is close to the value obtained in the linear case (test 3).

In figure 13, it was observed that the original Gaussian pulse of u separates into two smooth structures. The taller is thinner and travels faster than the shorter one. At the final instant of simulation, we invert these waves to initialize a new computation (top of figure 14). In the inviscid case, we observe that the two waves interact like classical solitons, exchanging their shape [16, 17]. After separation, each wave has again the original form, though shifted in location from where they would be without interaction. These behaviors are qualitatively maintained in the viscous case, even if it is less clear due to the attenuation of waves.

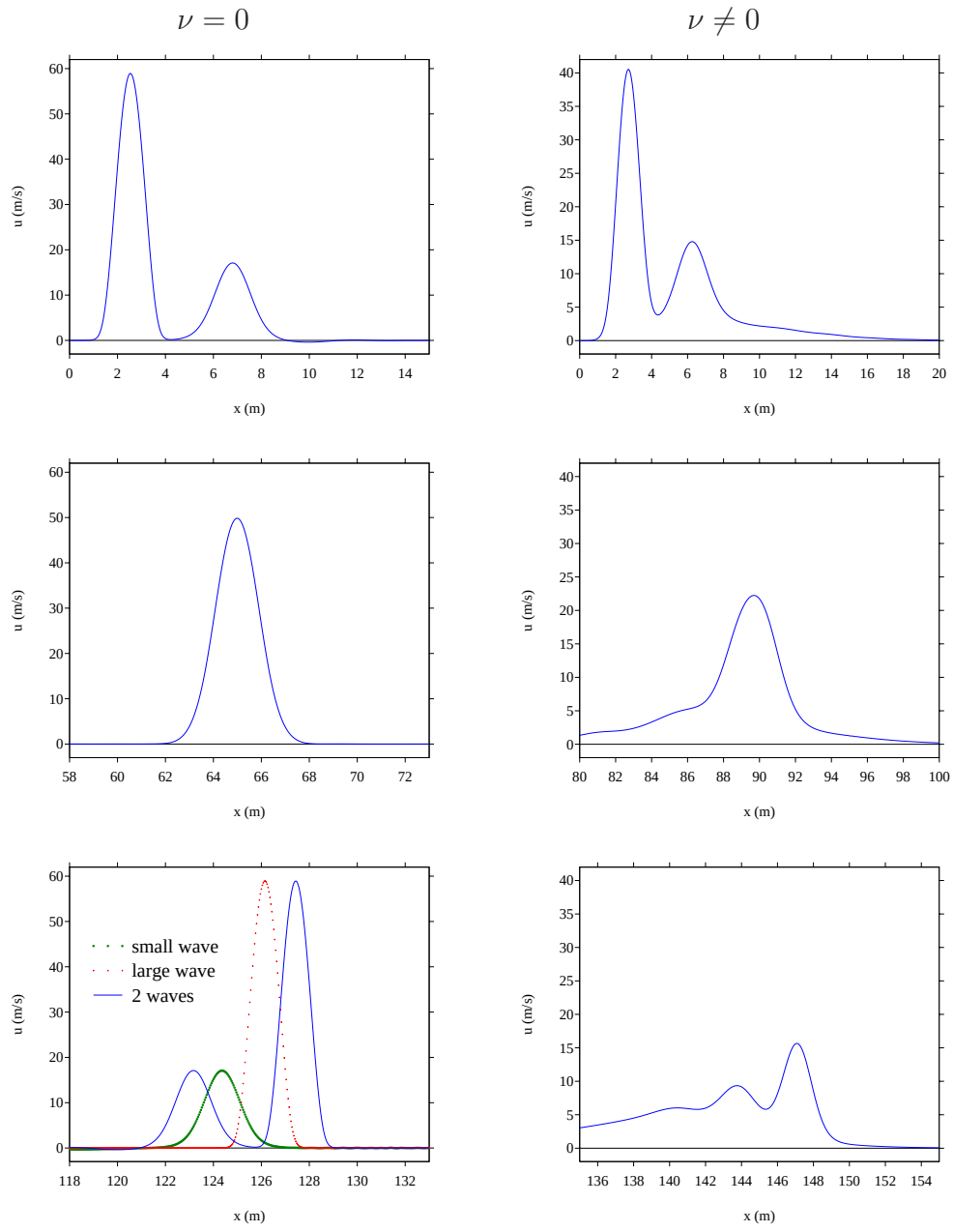

Figure 14: test4. Nonlinear coupled system, with a Gaussian pulse, $K = 0.5$ and $\Omega = 16$. Collision between two solitary waves. In green and red: location of the waves if they were alone.

6. Conclusion

We have considered nonlinear acoustic waves in a tube with an array of resonators. Various challenging physical features are involved: nonlinearity due to the amplitude of waves, dispersion induced by the resonators, and fractional derivatives of order -1/2 and 3/2 due to viscous losses.

Our original contribution was to propose an efficient and accurate numerical modeling of this configuration. Some tools are standard (TVD scheme for the nonlinear hyperbolic part), some others are more recent (diffusive representation of fractional derivatives). To our knowledge, it is the first time that diffusive representation is considered together with advection-Burgers equation. Lastly, a splitting strategy has ensured an optimal CFL condition for an explicit scheme. The proposed approach is computationaly efficient: the CFL stability condition is only governed by the nonlinearity (as in the usual advection-Burgers equation), and a minimum number of supplementary arrays is required to discretize the fractional derivatives.

This work has been motivated by the experimental configuration shown in figure 1, previously used in the linear regime of propagation [25, 26], and currently investigated in the nonlinear regime. Our objective was to provide an efficient and accurate numerical modeling, validating (or not) the model (4) and the underlying hypotheses. Numerical experiments have shown that the viscous effects do not modify qualitatively the wave phenomena. Consequently, the theoretical predictions done in the inviscid case about the existence of acoustic solitons are also obtained in the viscous case [29].

A first extension of this work concerns the coefficients of the diffusive representation. In some linear problems, is is possible to determine the time evolution of the energy and to prove that this energy decreases as soon as all the coefficients $\mu_l > 0$ ($l = 1 \cdots N$) of the diffusive representations of the fractional derivatives are positive [13, 6]. Therefore methods leading to positive $\mu_l > 0$ are usually prefered. As already pointed out, it is the case for the Laguerre method but not for the optimization method we use. One perspective is to develop an alternative method ensuring the positivity of the coefficients μ_l. A first possibility is to use an analytical method consisting in appoximating the function $\chi(\omega)$ by rational fractions. A second approach is to use an optimization process with a positivity constraint, for instance a Shor algorithm [24] initialized with the results from the Laguerre method. In the case of propoelasticity [3], this method has led to 10 up to 100 times more accurate results.

From a physical point of view, the dissipation effects require also further investigations. To get solitons, one needs to have $\Omega \gg 1$ (20), which implies $\omega \ll \omega_0$. In this regime, the dispersion analysis indicates that the attenuation is quite low (left part of figure 3). On the contrary, a high attenuation of waves is observed experimentally. A possible explanation of this mismatch is that some mechanisms of attenuation are not incorporated in the model. A good candidate is given by turbulence and nonlinear losses in the resonators. To account for these losses, a nonlinear theory for the response of the resonators has been proposed in the appendix of [29]. Equation (4b) with notations (5) should be replaced by the nonlinear fractional ODE

$$\begin{aligned} \frac{\partial^2 p}{\partial t^2} + \frac{2\sqrt{\nu}}{r}\frac{L^{'}}{L_e}\frac{\partial^{3/2} p}{\partial t^{3/2}} + \omega_e^2\, p - \frac{\gamma-1}{2\,\gamma}\frac{1}{p_0}\frac{\partial^2 (p)^2}{\partial t^2} \\ + \frac{V}{B\,L_e\,\rho_0\,a_0^2}\left|\frac{\partial p}{\partial t}\right|\frac{\partial p}{\partial t} = \omega_e^2\,\frac{\gamma\,p_0}{a_0}\,u, \end{aligned} \tag{57}$$

with the new parameters

$$L^{'} = L + 2\,r, \qquad L_e = L + \eta, \qquad \omega_e^2 = \frac{L}{L_e}\,\omega_0^2, \tag{58}$$

where η is determined experimentally ($\eta \approx 0.82\,r$). The term $\partial^2 (p)^2 / \partial t^2$ models the nonlinearity due to the adiabatic process in the cavity, whereas the semi-empirical term depending on the sign of $\partial p/\partial t$ accounts from the jet loss resulting from the difference in flow patterns on the inflow and outflow sides of the throat [29]. A more sophisticated numerical method must be developed to integrate (57).

A last extension of our work concerns the case where the height H of each resonator may vary with position, leading to variable coefficients in (4). Numerically, it requires to build smooth functions $e(x)$, $g(x)$ and $h(x)$, for instance with cubic splines. The exponential of $\mathbf{S}$ in (38) and (52) needs to be computed at each grid node and at each time step, which increases the computational cost, but no other modifications are required. It will allow to investigate numerically the propagation of acoustic solitons in random media [11]. This topic is a subject of intense research in various fields of physics, with possible applications in the transport of information.

Acknowledgments. This study has been initiated with Agnès Maurel (ESPCI, France), Olivier Richoux and Vincent Pagneux (LAUM, France), and has received financial support from the Agence Nationale de la Recherche through the grant ANR ProCoMedia, project ANR-10-INTB-0914. Pierre Haldenwang (AMU, France) is thanked for his insights about hyperbolic equations.

[1] C. Birk, C. Song, *An improved non-classical method for the solution of fractional differential equations*, Comput. Mech., 46 (2010), 721-734.

[2] E. Blanc, G. Chiavassa, B. Lombard, *Biot-JKD model: simulation of 1D transient poroelastic waves with fractional derivatives*, J. Comput. Phys., 237 (2013), 1-20.

[3] E. Blanc, G. Chiavassa, B. Lombard, *Numerical modeling of anisotropic poroelastic waves in the full range of frequencies*, to be submitted (2013).

[4] L. Brillouin, P. Parodi, *Propagation des Ondes dans les Milieux Périodiques*, Masson-Dunod, Paris (1956).

[5] W. Chester, *Resonant oscillations in closed tubes*, J. Fluid Mech., 18 (1964), 44-64.

[6] J. F. Deü, D. Matignon, *Simulation of fractionally damped mechanical systems by means of a Newmark-diffusive scheme*, Comput. Math. App., 59 (2010), 1745-1753.

[7] M. Dehghan, *Weighted finite difference techniques for the one-dimensional advection-diffusion equation*, Appl. Math. Comput., 147 (2004), 307-319.

[8] K. Diethelm, *An investigation of some nonclassical methods for the numerical approximation of Caputo-type fractional derivatives*, Numer. Algor., 47 (2008), 361-390.

[9] B.P. Flannery, W.H. Press, S.A. Teukolsky, W.T. Vetterling, *Numerical Recipes in C: the Art of Scientific Computing*, Second Edition, Cambridge University Press (1992).

[10] A. C. Galucio, J. F. Deü, S. Mengué, F. Dubois, *An adaptation of the Gear scheme for fractional derivatives*, Comput. Methods Appl. Mech. Engrg., 195 (2006), 6073-6085.

[11] J. Garnier, *Asymptotic transmission of solitons through random media*, SIAM J. Appl. Math., 58-6 (1998), 1969-1995.

[12] J.P. Groby, C. Tsogka, *A time domain method for modeling viscoacoustic wave propagation*, J. Comput. Acoust., 14-2 (2006), 201-236.

[13] H. Haddar, J. R. Li, D. Matignon, *Efficient solution of a wave equation with fractional-order dissipative terms*, J. Comput. Appl. Math., 2-6 (2010), 2003-2010.

[14] H. Holden, K. H. Karlsen, N. H. Risebro, T. Tao, *Operator splitting for the KDV equation*, Math. Comput., 80 (2011), 821-846.

[15] R. J. LeVeque, *Numerical methods for conservation laws*, 2nd edition, Birkhäuser-Verlag, 1992.

[16] R. J. LeVeque, D. H. Yong, *Phase plane behavior of solitary waves in nonlinear layered media*, 9th International Conference on Hyperbolic Problems: Theory, Numerics, Applications. Springer, 2002.

[17] R. J. LeVeque, D. H. Yong, *Solitary waves in layered nonlinear media*, SIAM J. Appl. Math., 63-5 (2003), 1539-1560.

[18] J. F. Lu, A. Hanyga, *Wave field simulation for heterogeneous porous media with singular memory drag force*, J. Comput. Phys., 208 (2005), 651-674.

[19] D. Matignon, *An introduction to fractional calculus*, Scaling, Fractals and Wavelets (Digital Signal and Image Processing Series), ISTE-Wiley, 2008.

[20] L. Menguy, J. Gilbert, *Weakly non-linear gas oscillations in air-filled tubes ; solutions and experiments*, Acustica, 86 (2000), 798-810.

[21] C. B. Moler, C. F. Van Loan, *Nineteen dubious ways to compute the exponential of a matrix, twenty-five years later*, SIAM Review, 45 (2003), 3-49.

[22] P. Monkewitz, N. M. Nguyen-Vo, *The response of Helmholtz resonators to external excitation. Part 1. Single resonators*, J. Fluid Mech., 151 (1985), 477-497.

[23] P. Monkewitz, *The response of Helmholtz resonators to external excitation. Part 2. Arrays of slit resonators*, J. Fluid Mech., 156 (1985), 151-166.

[24] A. Rekik, R. Brenner, *Optimization of the collocation inversion method for the linear viscoelastic homogenization*, Mech. Res. Comm., 38 (2011), 305-308.

[25] O. Richoux, C. Depollier, J. Hardy, *Propagation of mechanical waves in a one-dimensional nonlinear disordered lattice*, Phys. Rev. E 73 (2006), 026611.

[26] O. Richoux, V. Tournat, T. Le Van Suu, *Acoustic wave dispersion in a one-dimensional lattice of nonlinear resonant scatterers*, Phys. Rev. E, 75-2 (2007), 026615.

[27] E. Sousa, *The controversial stability analysis*, Appl. Math. Comput., 145 (2003), 777-794.

[28] N. Sugimoto, *Burgers equation with a fractional derivative; hereditary effects on nonlinear acoustic waves*, J. Fluid. Mech., 225 (1991), 631-653.

[29] N. Sugimoto, *Propagation of nonlinear acoustic waves in a tunnel with an array of Helmholtz resonators*, J. Fluid. Mech., 244 (1992), 55-78.

[30] N. Sugimoto, *Acoustic solitary waves in a tunnel with an array of Helmholtz resonators*, J. Acoust. Soc. Am., 99-4 (1996), 1971-1976.

[31] N. Sugimoto, M. Masuda, J. Ohno, D. Motoi, *Experimental demonstration of generation and propagation of acoustic solitary waves in a air-filled tube*, Phys. Rev. Lett., 83-20 (1999), 4053-4056.

[32] N. Sugimoto, M. Masuda, K. Yamashita, H. Horimoto, *Verification of acoustic solitary waves*, J. Fluid. Mech., 504 (2004), 271-299.

[33] T. Tao, *Why are solitons stable ?*, Bull. Amer. Math. Soc. 46 (2009), 1-33.

[34] M. Toda, *Nonlinear waves and solitons*, Kluwer Academic Publisher Group, 1989.

[35] L. Yuan, O. M. Agrawal, *A numerical scheme for dynamic systems containing fractional derivatives*, J. Vibr. Acoust., 124 (2002), 321-324.